The crystal structure of $MoO_2(O_2)(H_2O)\cdot H_2O$

Joel W. Reid,[1,a] James A. Kaduk,[2] and Lidia Matei[3]
[1]*Canadian Light Source, 44 Innovation Boulevard, Saskatoon, SK, S7N 2V3, Canada*
[2]*Illinois Institute of Technology, 3101 S. Dearborn St., Chicago, Illinois, 60616*
[3]*Canadian Isotope Innovations Corp., 232-111 Research Drive, Saskatoon, SK, S7N 3R2, Canada*

(Received 26 August 2018; accepted 27 December 2018)

The crystal structure of $MoO_2(O_2)(H_2O)\cdot H_2O$ has been solved using parallel tempering with the FOX software package and refined using synchrotron powder diffraction data obtained from beamline 08B1-1 at the Canadian Light Source. Rietveld refinement, performed with the software package GSAS, yielded monoclinic lattice parameters of $a = 17.3355(5)$ Å, $b = 3.83342(10)$ Å, $c = 6.55760(18)$ Å, and $\beta = 91.2114(27)°$ ($Z = 4$, space group $I2/m$). The structure is composed of double zigzag molybdate chains running parallel to the b-axis. The Rietveld refined structure was compared with density functional theory (DFT) calculations performed with CRYSTAL14, and shows comparable agreement with two DFT optimized structures of similar energy, which differ by the location of the molybdate coordinated water molecule. The true structure is likely a disordered combination of the two DFT optimized structures. © *2019 International Centre for Diffraction Data*.
[doi:10.1017/S0885715619000095]

Key words: molybdenum peroxide, powder diffraction, structure solution, density functional theory

I. INTRODUCTION

Preparation of the medical isotope technetium-99m (^{99m}Tc, daughter isotope of ^{99}Mo) using non-traditional methods such as linear accelerator (LINAC) production (Hoedl and Updegraff, 2015) has taken on increased importance. The recent shuttering of the National Research Universal (NRU) nuclear reactor facility at Chalk River (Lougheed, 2017), uncertainty in the supply chain security for ^{99}Mo (Van Noordan, 2013), and desire for migration to production routes that do not require highly enriched uranium have increased the emphasis on developing alternative techniques for isotope production (Lyra *et al*., 2011; Wolterbeek *et al*., 2014; Welsh *et al*., 2015).

Chemistry development for target processing and Mo recycling related to LINAC production of ^{99}Mo recently led to the structural characterization of two molybdate compounds (Reid *et al*., 2017, 2018). The phase described in this work appears comparable to a hydrated molybdenum peroxide phase documented previously in the Powder Diffraction File (ICDD, 2016), $H_2MoO_5\cdot H_2O$ (PDF entry 00-041-0060), without determination of the crystal structure. This work describes the crystal structure and provides a reflection list based on the final Rietveld refinement for phase identification.

II. EXPERIMENTAL

A specimen of molybdenum processing powder supplied by Canadian Isotope Innovation Corp. was examined as-synthesized. The specimen was mounted in a 0.5 mm ID Kapton capillary, which was sealed at both ends with adhesive.

Powder X-ray diffraction (PXRD) patterns were collected using a Canadian Macromolecular Crystallography Facility beamline (08B1-1, Fodje *et al*., 2014) at the Canadian Light Source (CLS). 08B1-1 is a bending magnet beamline with a Si (111) double-crystal monochromator. Two-dimensional (2D) data were obtained using a Rayonix MX300HE detector with an active area of 300 mm × 300 mm. The patterns were collected at an energy of 18 keV ($\lambda = 0.68880$ Å) and a sample-detector distance of 250 mm.

The 2D PXRD patterns were calibrated and integrated using the GSASII software package (Toby and Von Dreele, 2013). The sample-detector distance, detector centering, and tilt were calibrated using a lanthanum hexaboride (LaB6) standard reference material (NIST SRM 660a LaB6) and the calibration parameters were applied to all patterns. After calibration, the 2D patterns were integrated to obtain standard powder diffraction patterns. A pattern collected from an empty Kapton capillary (using the same conditions) was subtracted from the sample data during integration.

Search/match phase identification performed with the Powder Diffraction File, PDF-4+ (ICDD, 2016), identified an indexed experimental pattern for $H_2MoO_5\cdot H_2O$ [PDF entry 00-041-0060, unit-cell parameters $a = 17.156(1)$ Å, $b = 3.8749(3)$ Å, $c = 6.5506(4)$ Å, $\beta = 90.832(4)°$, space group $I2/m$]. Multiple remaining Bragg reflections could not be identified with search/match phase identification, but could be indexed with a number of unit cells using DICVOL06 (Boultif and Louer, 2004). After testing these unit cells, a monoclinic cell with lattice parameters $a = 10.2187$ Å, $b = 22.0825$ Å, $c = 8.9545$ Å, and $\beta = 97.500°$ ($M_{20} = 9.1$, $F_{20} = 40.4$) was used for subsequent Le Bail refinement (Le Bail *et al*., 1988) for this unknown phase. Figure 1 illustrates the low-angle Bragg reflections for both the main $MoO_2(O_2)(H_2O)\cdot H_2O$ phase and the unknown monoclinic impurity phase.

[a]Author to whom correspondence should be addressed. Electronic mail: joel.reid@lightsource.ca

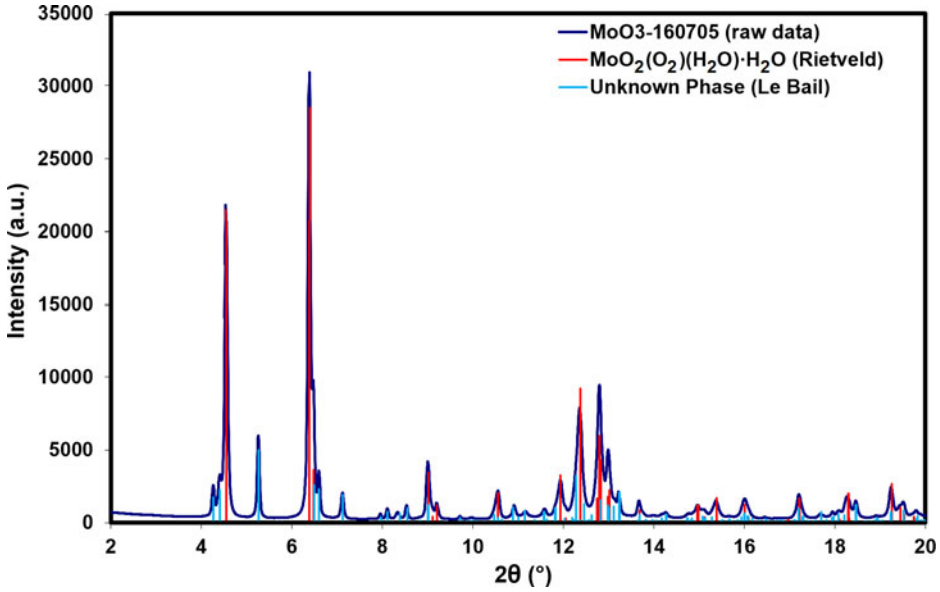

Figure 1. (Color online) A plot of the raw data for the sample vs. the Bragg reflections for the $MoO_2(O_2)(H_2O)\cdot H_2O$ phase obtained from Rietveld refinement and the unknown phase obtained from Le Bail refinement.

TABLE I. The crystal data, data collection, and refinement parameters obtained for $MoO_2(O_2)(H_2O)\cdot H_2O$.

Crystal data	
Formula, Z	$MoO_2(O_2)(H_2O)\cdot H_2O$, $Z = 4$
Molecular mass (M_r)	195.986 g mol^{-1}
Symmetry, space group	Monoclinic, $I2/m$ (12)
Unit-cell parameters	$a = 17.3355(5)$ Å, $b = 3.83342(10)$ Å, $c = 6.55760(18)$ Å, $\beta = 91.2114(27)°$
Volume	435.684(28) Å^3
Density (ρ_{calc})	2.988 g cm^{-3}
Data collection	
Beamline	CLS 08B1-1
Monochromator	Si (111) double crystal monochromator
Detector	Rayonix MX300HE (300 mm × 300 mm)
Specimen mounting	0.5 mm Kapton capillary
Collection mode	Transmission
Wavelength	$\lambda = 0.68880$ Å
Collection range, step size	2–39° (2θ), 0.005°/step
Refinement	
Number of data points	7400
Background correction	Nine-term Chebyschev polynomial
Number of refined parameters	40
R_p	0.0369
R_{wp}	0.0573
R_{exp}	0.0338
χ^2	2.90

TABLE II. The Rietveld refined crystal structure of $MoO_2(O_2)(H_2O)\cdot H_2O$ with lattice parameters $a = 17.3355(5)$ Å, $b = 3.83342(10)$ Å, $c = 6.55760(18)$ Å, and $\beta = 91.2114(27)°$.

Atom	*x/a*	*y/b*	*z/c*	Wyckoff	U_{iso} (Å^2)
Mo1	0.17913(8)	0.5	−0.34162(21)	4i	0.0468(5)
O2	0.1778(4)	0.5	−0.0324(11)	4i	0.0262(11)
O3	0.1953(4)	0	−0.2959(10)	4i	0.0262(11)
O4	−0.27333(33)	0	−0.1368(11)	4i	0.0262(11)
O5	0.08653(21)	0.3373(9)	−0.4132(7)	8j	0.0262(11)
O6	−0.05513(33)	0	−0.1834(11)	4i	0.0262(11)

All atoms were refined with fixed site occupancies of 1.

A reduced cell search of the PDF using the cell for the main $H_2MoO_5\cdot H_2O$ phase identified a hydrated tungsten peroxide, $WO_2(O_2)(H_2O)_{2.66}$ [unit-cell parameters $a = 12.4110(7)$ Å, $b = 3.8717(3)$ Å, $c = 10.1405(6)$ Å, $\beta = 117.553(3)°$, space group $C2/m$], as a potentially analogous structure (PDF entry 04-011-4401, Pecquenard *et al.*, 1998). However, preliminary

https://doi.org/10.1017/S0885715619000095 Published online by Cambridge University Press

TABLE III. The DFT optimized crystal structures of $MoO_2(O_2)(H_2O)\cdot H_2O$ with fixed lattice parameters $a = 17.3362$ Å, $b = 3.8336$ Å, $c = 6.5580$ Å, and $\beta = 91.2132°$.

	x/a		*y/b*		*z/c*	
Atom	DFT-O2	DFT-O4	DFT-O2	DFT-O4	DFT-O2	DFT-O4
Mo1	0.18418	0.17106	0.5	0.5	−0.36669	−0.23913
O2	0.14338	0.15886	0.5	0.5	−0.03125	0.01400
O3	0.20780	0.20723	0	0	−0.28443	−0.27674
O4	−0.28284	−0.30327	0	0	−0.10428	−0.08778
O5	0.07982	0.07147	0.31527	0.31490	−0.41935	−0.33521
O6	−0.05901	−0.08328	0	0	−0.19195	−0.24698
H7	0.11798	0.17439	−0.29525	−0.30009	0.02434	0.34045
H8	−0.05328	−0.05017	0.19064	0.19282	−0.28809	−0.28289

The structures differ by the placement of H7 with a water molecule on either the O2 or O4 sites (DFT-O2 and DFT-O4, respectively).

Rietveld refinements based on this model were unsuccessful and the structure was ultimately solved using parallel tempering with the FOX software package (Favre-Nicolin and Černý, 2002) using the unit-cell and space group setting from PDF entry 00-041-0060. Roughly 30 sets of parallel tempering with 2×10^6 trials/set resulted in multiple comparable solutions with cost functions of ∼50 000, reflecting the presence of unaccounted for Bragg reflections from the impurity phase.

Rietveld refinements of the crystal structure were performed with both the GSAS/EXPGUI programs (Toby, 2001; Larson and Von Dreele, 2004) and FullProf (Rodriguez-Carvajal, 2001); the results described here were obtained with GSAS/EXPGUI using the pseudo-Voigt reflection profile of

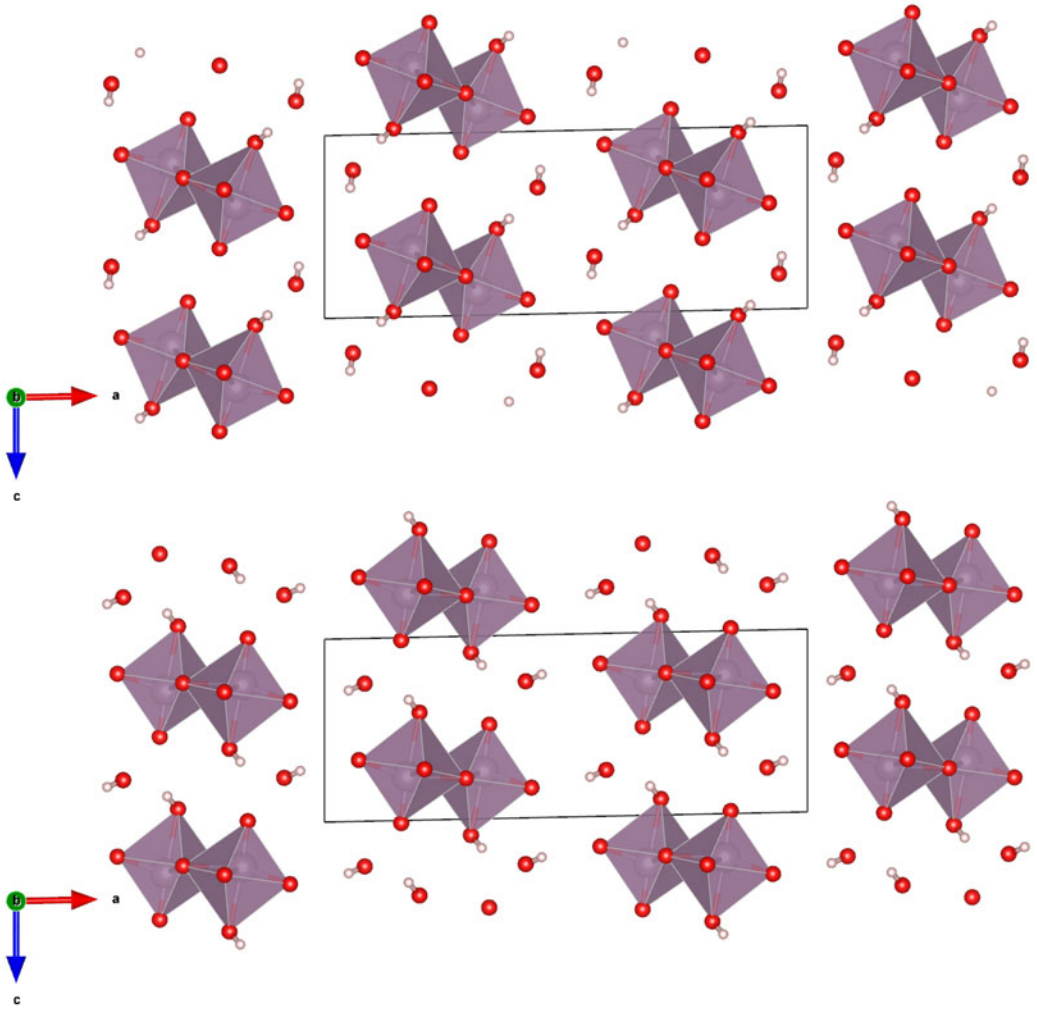

Figure 2. (Color online) The DFT optimized crystal structures of $MoO_2(O_2)(H_2O)\cdot H_2O$, viewed along the *b*-axis with water hydrogen atoms associated with O2 (top) and O4 (bottom). The polyhedra and atom types can be identified by color including MoO_6 (purple octahedra), hydrogen (pink), and O (red). The unit cell is outlined in black. The figure was prepared with VESTA (Momma and Izumi, 2011).

https://doi.org/10.1017/S0885715619000095 Published online by Cambridge University Press

Thompson *et al.* (1987). Anomalous scattering factors were interpolated from the tables of Sasaki (1989). The background was modeled using a nine-term Chebyshev polynomial. Positional parameters were refined with no restraints for the Mo and O atoms, while isotropic displacement parameters were refined for the Mo and constrained as equal for all the O atoms.

The crystal data, data collection, and refinement details are summarized in Table I.

Two density functional geometry optimizations (using a fixed experimental unit cell) were carried out using CRYSTAL14 (Dovesi *et al.*, 2014), with the hydrogen (H7) for the molybdate coordinated water placed at either O2 or O4 (denoted DFT-O2 and DFT-O4, respectively). The basis sets were obtained from the literature for the H and O (Gatti *et al.*, 1994) and Mo atoms (Cora *et al.*, 1997). The calculation was run on eight 2.1 GHz Xeon cores (each with 6 Gb RAM) of a 304-core Dell Linux cluster at the Illinois Institute of Technology (IIT), used 8 *k*-points and the B3LYP functional.

III. RESULTS AND DISCUSSION

The Rietveld refined atomic coordinates obtained with GSAS for $MoO_2(O_2)(H_2O)\cdot H_2O$ are given in Table II, while density functional theory (DFT) optimized atomic coordinates are given in Table III for two models with molybdate coordinated water molecules at either O2 or O4 (DFT-O2 and DFT-O4, respectively). The DFT optimized models are illustrated for comparison along the *b*-axis and *c*-axis in Figures 2 and 3, respectively. The root-mean square (RMS) Cartesian displacement between the two DFT models for the heavy (non-hydrogen) atoms is 0.0125 Å, and the structures differ in energy by 0.06 kcal mol^{-1}, making them essentially indistinguishable except for the placement of H7 associated with the molybdate coordinated water molecule.

The RMS Cartesian displacement between the Rietveld refined atomic coordinates and the two DFT models are 0.2437 and 0.2446 Å, respectively (for DFT-O2 and DFT-O4). The RMS differences are higher than those obtained for previous molybdate structures refined using comparable data acquisition (Reid *et al.*, 2017, 2018). This probably reflects increased uncertainty in the correct Bragg intensities for the main phase because of the use of Le Bail refinement for the unknown impurity phase observed in the current data. The final Rietveld refinement is illustrated in Figure 4. While the monoclinic unit cell used for the Le Bail refinement of the impurity phase was the optimal cell of five unit cells which were tested, it may not be the correct cell, and the chemistry of the impurity phase remains unknown. An offset plot comparing the observed pattern to the calculated patterns for both phases is illustrated in Figure 5.

Similar to the previously characterized $MoO_2(O_2)H_2O$ structure (Reid *et al.*, 2018), this structure is characterized by double zigzag molybdate chains running parallel to the *b*-axis. The additional water molecule between molybdate chains in the current compound results in a less densely packed structure compared with $MoO_2(O_2)H_2O$ (the calculated densities are 2.988 and 3.511 g cm^{-3}, respectively). The bond valence sum (Brown, 2002) for Mo1 in the Rietveld refined structure is 6.181(28), while the Mo-O bond lengths are shown for both the Rietveld and DFT optimized structures in Table IV. The Mo1-O2 and Mo1-O4 bond lengths for the Rietveld refined model fall between the values for the two DFT optimized models, likely suggesting that the molybdate coordinated water molecules are disordered over the O2 and O4 sites. Attempts were made to refine the

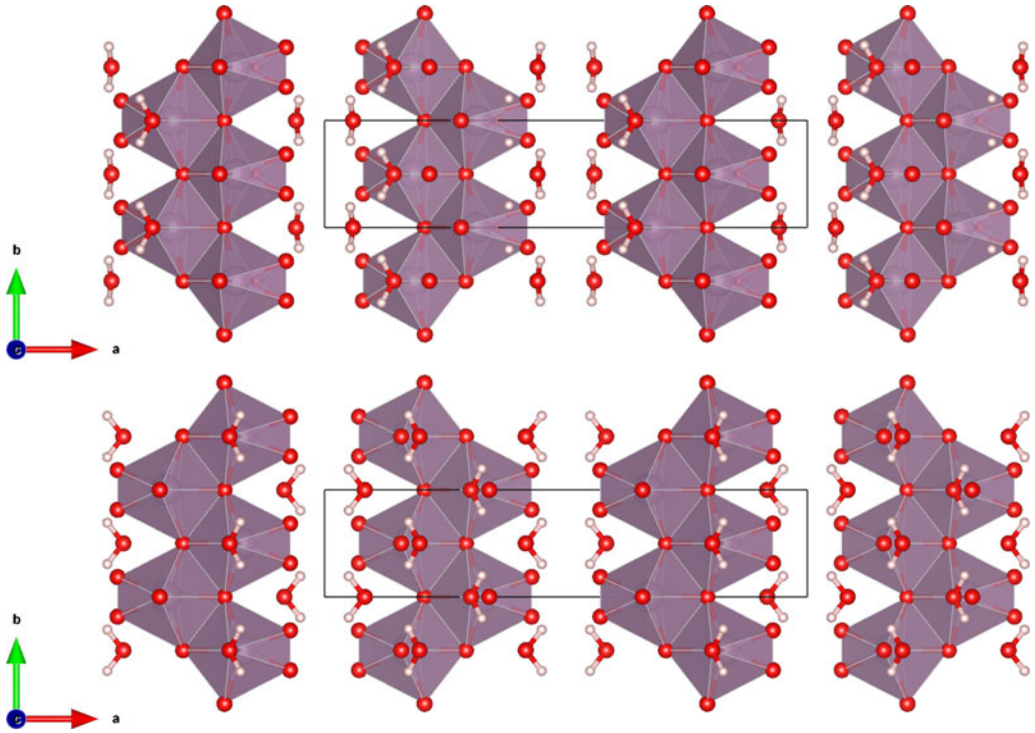

Figure 3. (Color online) The DFT optimized crystal structures of $MoO_2(O_2)(H_2O)\cdot H_2O$, viewed along the *c*-axis with water hydrogen atoms associated with O2 (top) and O4 (bottom). The polyhedra and atom types can be identified by color including MoO_6 (purple octahedra), hydrogen (pink), and O (red). The unit cell is outlined in black. The figure was prepared with VESTA (Momma and Izumi, 2011).

https://doi.org/10.1017/S0885715619000095 Published online by Cambridge University Press

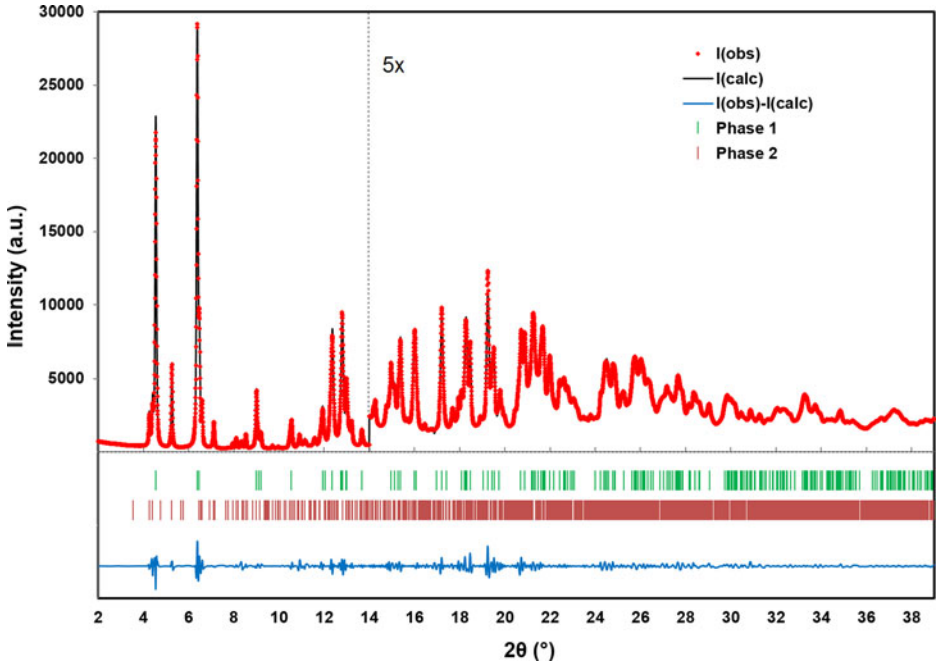

Figure 4. (Color online) A plot illustrating the final Rietveld refinement of $MoO_2(O_2)(H_2O)\cdot H_2O$ (phase 1) obtained with GSAS. Phase 2 refers to the unknown monoclinic phase refined with Le Bail refinement. The data are magnified by a factor of 5 for the region above 14° (2θ).

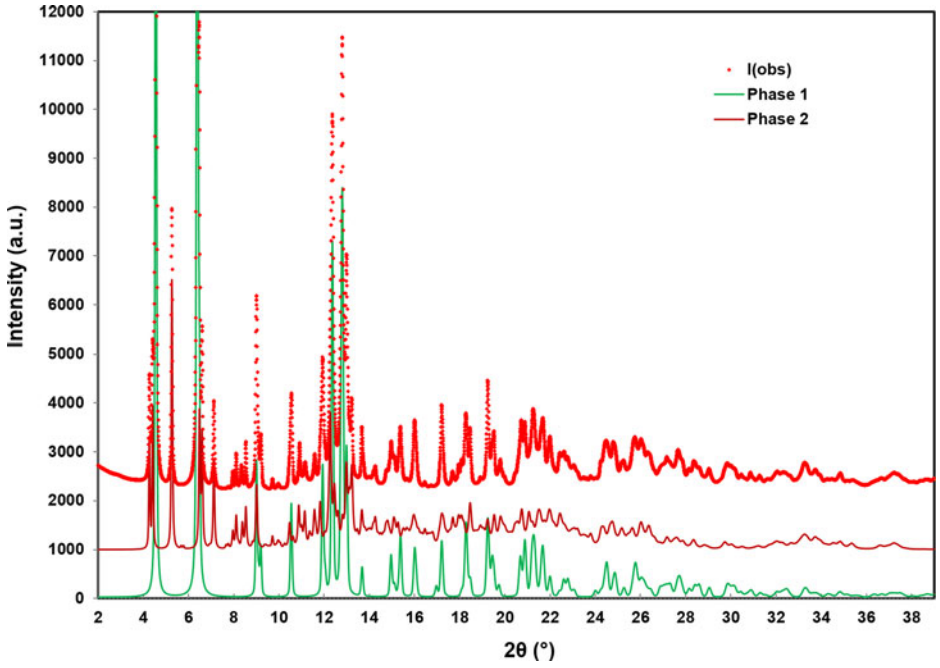

Figure 5. (Color online) An offset plot comparing the observed data to the Rietveld refined pattern of $MoO_2(O_2)(H_2O)\cdot H_2O$ (phase 1) and the Le Bail refined pattern for the unknown monoclinic phase (phase 2).

structure starting from the DFT optimized models with the molybdate coordinated water molecule situated on (1) O2, (2) O4, and (3) split between the two sites, but the results were ultimately inconclusive.

The hydrogen bonds observed in the two DFT optimized structures are summarized in Table V. The hydrogen bond energies were calculated from the overlap populations using the correlation function of Rammohan and Kaduk (2018). Both water hydrogens participate in discrete hydrogen bonds, with graph sets D1,1(2).

TABLE IV. The Mo-O bond lengths obtained from the Rietveld refinement and DFT optimized structures.

Bond	Rietveld (Å)	DFT-O2 (Å)	DFT-O4 (Å)
Mo1-O2	2.028(7)	2.325	1.678
Mo1-O3	1.9591(13)	2.031	2.033
Mo1-O3	1.9591(13)	2.031	2.033
Mo1-O3	2.339(6)	2.100	2.110
Mo1-O4	2.120(6)	1.671	2.339
Mo1-O5	1.776(4)	1.967	1.958
Mo1-O5	1.776(4)	1.967	1.958

https://doi.org/10.1017/S0885715619000095 Published online by Cambridge University Press

TABLE V. Hydrogen bonds observed in the $MoO_2(O_2)(H_2O)\cdot H_2O$ DFT optimized structures and their parameters as determined by the DFT modeling.

H-bond	D-H (Å)	H···A (Å)	D···A (Å)	D-H···A (°)	Overlap (*e*)	E (kcal mol^{-1})
			DFT-O2			
O2-H7···O6	0.975	1.893	2.837	162.3	0.040	10.9
O6-H8···O5	0.972	2.021	2.837	140.3	0.023	8.3
O6-H8···O5	0.972	2.525	3.103	118.0	0.005	3.9
			DFT-O4			
O4-H7···O6	0.975	2.038	2.937	152.4	0.034	10.1
O4-H7···O2	0.975	2.284	2.679	103.1	0.005	3.9
O6-H8···O5	0.968	2.194	3.009	141.1	0.017	7.1

A Bragg reflection list was prepared by summing reflections closer than 0.02° 2θ as multiple reflections and assigning a weighted average reflection position, then including all reflections with relative integrated intensities of 0.5% or greater up to 39° 2θ. The Bragg reflection list and raw data are contained in a crystallographic information file (CIF) in the online Supplementary material, along with individual CIF files for the Rietveld refined and DFT optimized structures.

SUPPLEMENTARY MATERIAL

The supplementary material for this article can be found at https://doi.org/10.1017/S0885715619000095.

ACKNOWLEDGEMENTS

The authors thank Andrey Rogachev for the use of the computing resources at the Illinois Institute of Technology. Research described in this paper was performed using beamline 08B1-1 at the Canadian Light Source, which is supported by the Canadian Foundation for Innovation, the Natural Sciences and Engineering Research Council of Canada, the National Research Council Canada, the Canadian Institutes of Health Research, the Government of Saskatchewan, Western Economic Diversification Canada, and the University of Saskatchewan.

Boultif, A. and Louer, D. (**2004**). "Powder pattern indexing with the dichotomy method," J. Appl. Crystallogr. **37**, 724–731.

Brown, I. D. (**2002**). *The Chemical Bond in Inorganic Chemistry: The Bond Valence Model* (Oxford University Press, New York).

Cora, F., Patel, A., Harrison, N. M., Roetti, C., and Catlow, C. R. A. (**1997**). "An ab-initio Hartree-Fock study of alpha-MoO3," J. Mater. Chem. **7**, 959–967.

Dovesi, R., Orlando, R., Erba, A., Zicovich-Wilson, C. M., Civalleri, B., Casassa, S., Maschio, L., Ferrabone, M., De La Pierre, M., D'Arco, P., Noel, Y., Causa, M., Rerat, M., and Kirtman, B. (**2014**). "CRYSTAL14: a program for the *ab initio* investigation of crystalline solids," Int. J. Quant. Chem. **114**, 1287–1313.

Favre-Nicolin, V. and Černý, R. (**2002**). "FOX, 'free objects for crystallography': a modular approach to *ab initio* structure determination from powder diffraction," J. Appl. Crystallogr. **35**, 734–743.

Fodje, M., Grochulski, P., Janzen, K., Labiuk, S., Gorin, J., and Berg, R. (**2014**). "08B1-1: an automated beamline for macromolecular crystallography experiments at the Canadian light source," J. Synchrotron Rad. **21**, 633–637.

Gatti, C., Saunders, V. R., and Roetti, C. (**1994**). "Crystal-field effects on the topological properties of the electron-density in molecular crystals – the case of urea," J. Chem. Phys. **101**, 10686–10696.

Hoedl, S. A. and Updegraff, W. D. (**2015**). "The production of medical isotopes without nuclear reactors or uranium enrichment," Sci. Global Sec. **23**, 121–153.

ICDD (**2016**). *PDF-4 + 2016 (Database)*. edited by Dr. S. Kabekkodu (International Centre for Diffraction Data, Newtown Square, PA, USA).

Larson, A. C. and Von Dreele, R. B. (**2004**). General Structure Analysis System (GSAS) (Report No. LAUR 86-748), Los Alamos National Laboratory, Los Alamos, NM.

Le Bail, A., Duroy, H., and Fourquet, J. L. (**1988**). "Ab-initio structure determination of LiSbWO6 by X-ray powder diffraction," Mater. Res. Bull. **23**, 447–452.

Lougheed, T. (**2017**). Canada's neutron scientists lament closure of world's oldest nuclear reactor. Science, http://www.sciencemag.org/news/2017/09/canada-s-neutron-scientists-lament-closure-world-s-oldest-nuclear-reactor.

Lyra, M., Charalambatou, P., Roussou, E., Fytros, S., and Baika, I. (**2011**). "Alternative production methods to face global molybdenum-99 supply shortage," Hell. J. Nucl. Med. **14**, 49–55.

Momma, K. and Izumi, F. (**2011**). "VESTA 3 for three-dimensional visualization of crystal, volumetric and morphology data," J. Appl. Crystallogr. **44**, 1272–1276.

Pecquenard, B., Castro-Garcia, S., Livage, J., Zavalij, P. Y., Whittingham, M. S., and Thouvenot, R. (**1998**). "Structure of hydrated tungsten peroxides $[WO_2(O_2)H_2O]\cdot nH_2O$," Chem. Mater. **10**, 1882–1888.

Rammohan, A. and Kaduk, J. A. (**2018**). "Crystal structures of alkali metal (Group 1) citrate salts," Acta Crystallogr. B **74**, 239–252.

Reid, J. W., Kaduk, J. A., and Olson, J. A. (**2017**). "The crystal structure of $Na(NH_4)Mo_3O_{10}\cdot H_2O$," Powder Diffr. **32**, 140–147.

Reid, J. W., Kaduk, J. A., and Matei, L. (**2018**). "The crystal structure of $MoO_2(O_2)\cdot H_2O$," Powder Diffr. **33**, 49–54.

Rodriguez-Carvajal, J. (**2001**). "Recent developments of the program FULLPROF," IUCR Newslett. **26**, 12–19.

Sasaki, S. (**1989**). *Numerical Tables of Anomalous Scattering Factors Calculated by the Cromer and Lieberman's Method*. KEK Report 88-14.

Thompson, P., Cox, D. E., and Hastings, J. B. (**1987**). Rietveld refinement of Debye-Scherrer synchrotron X-ray data from $A1_20_3$," J. Appl. Crystallogr. **20**, 79–83.

Toby, B. H. (**2001**). "EXPGUI, a graphical user interface for GSAS," J. Appl. Crystallogr. **34**, 210–213.

Toby, B. H. and Von Dreele, R. B. (**2013**). "GSAS II: the genesis of a modern open-source all-purpose crystallography software package," J. Appl. Crystallogr. **46**, 544–549.

Van Noorden, R. (**2013**). "The medical testing crisis," Nature **504**, 202–204.

Welsh, J., Bigles, C. I., and Valderrabano, A. (**2015**). "Future U.S. supply of Mo-99 production through fission based LEU/LEU technology," J. Radioanal. Nucl. Chem. **305**, 9–12.

Wolterbeek, B., Kloosterman, J. L., Lathouwers, D., Rohde, M., Winkelman, A., Frima, L., and Wols, F. (**2014**). "What is wise in the production of ^{99}Mo? A comparison of eight possible production routes," J. Radioanal. Nucl. Chem. **302**, 773–779.